Supplement of

Atmospheric Evolution of Molecular Weight Separated Brown Carbon from Biomass Burning

J.P.S. Wong et al.

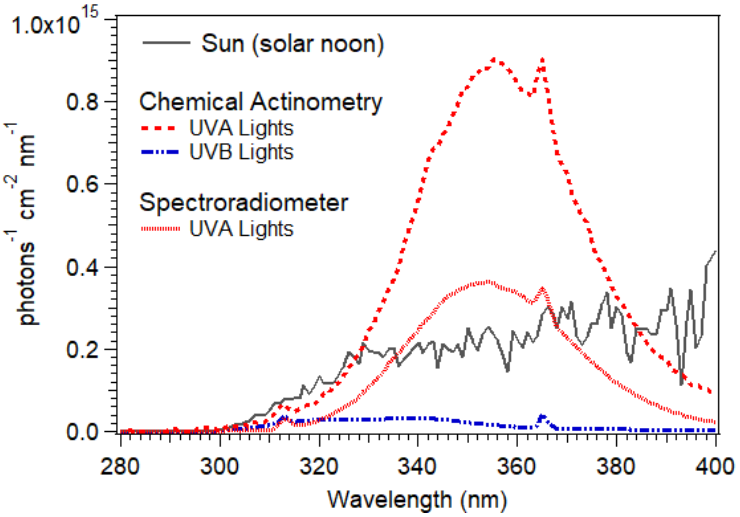

Figure S1. Measured photon flux in the photoreactor using chemical actinometry (dash lines) and spectroradiometer (solid line) for UVB (blue) and UVA lights (red; Wong et al., 2017). The actinic flux for a clear-sky summer day (black line) is included for comparison. The actinic flux was obtained from the National Center for Atmospheric Research (NCAR) "Quick TUV Calculator," available at http://cprm.acom.ucar.edu/Models/TUV/Interactive_TUV/ using the following parameters: Solar Zenith Angle = 0 deg, overhead ozone of 300 Dobson units, surface albedo of 0.1 and at 0 km attitude.

Section S1. OH Quantification Experiments

The following procedure for OH quantification using benzoate as a radical scanvenger was adapted from Zhou and Mopper (1990) and Anatasio and McGregor (2001). Sodium benzoate (0.1 – 1.0 µM; Sigma Aldrich) was added to WS wood smoke BrC extract solution with and without 1.5mM H_2O_2, in multiple 2 mL borosiliciate glass vials (sealed with Telfon-lined caps). The resulting vials were illuminated up to 18 hours in the photoreactor (equipped with 16 UVB lights), where at different times, a sample vial was removed and acidifed prior to injection with 2 drops of 1.0 M H_3PO_4 (Sigma Aldrich), to determine the concentration of *p*-HBA, using an High Performance Liquid Chromatrography (HPLC) system (GP40, Dionex), equipped with a C-18 column (Waters Symmetry®, 5 µm pore size, 4.6 mm diameter and 150 mm length), coupled to an UV/VIS spectrometer. The UV/VIS spectrometer consists of a liquid capillary waveguide (10 cm optical pathlength, World Precision Instrument), a deuterium tungsten halogen light source (DT-Mini-B, Ocean Optics), and an absorption spectrometer (USD4000, Ocean Optics). A two-solvent (A: acidified water at pH 2, using phosphate buffer; B: acetonitrile) multistep gradient elution was used to separate *p*-HBA from other isomers of hydroxybenzoic acid at a flow rate of 1.2 mL min^{-1}, as follows: isocratic at 80% A for 6.5 min, 80 to 50% A for 3.5 min; isocratic at 50% A for 1 min; 50% to 20% A in 4.5 min;

and then 20% to 80% A in 4.5 min. Absorption at λ = 256 nm were monitored for the detection of *p*-HBA (retention time, t_r =3.15 min). The response was calibrated by spiking *p*-HBA to WS BrC solution at various concentrations (i.e., standard addition method). The detection limit for *p*-HBA was determined to be ~ 200 nM, due to the absorbance at λ = 256 nm by BrC samples with the same elution time as *p*-HBA. We note that after only 30 min. of UVB irradiation, the observed production of *p*-HBA in WS BrC samples with 1.5 mM H_2O_2, is ten times of the detection limit. For each benzoate concentration, the formation rate of *p*-HBA ($R_{benzoate}$) was determined.

From the linear regression slope and y-intercept of the plot of 1/benzoate formation rate vs 1/benzoate concentration (Figure S3), two quanitites can be determined: the production rate of OH (P_{OH}, equation 1); and the apparent first-order rate constant of the reaction of BrC with OH (k'_{BrC}, equation 2):

$$P_{OH} = \text{y-intercept} \times Y_{pHBA} \quad (1)$$

$$k'_{BrC} = k_{benzoate} \times (\text{slope/y-intercept}) \quad (2)$$

where $k_{benzoate}$ is the reaction rate constant of benzoate with OH (5.9×10^9 M^{-1} s^{-1}; (Ross et al., 1994), and Y_{pHBA} is the yield of *p*-HBA from the reaction of benzoate with OH (0.17; Anastasio and McGregor, 2001). From these determined values, the steady-state concentration of OH ($[OH]_{ss}$) can be determined, as the OH production rate equals to the consumption rate by all OH scanvengers, which are WS BrC (R_{BrC}) and benzoate (R_{BrC}):

$$P_{OH} = R_{BrC} + R_{benzoate} \quad (3)$$

In which,

$$R_{BrC} = k'_{BrC}\,[OH]_{ss} \quad (4)$$

$$R_{benzoate} = k_{benzoate}[benzoate][OH]_{ss} \quad (5)$$

We note that the OH quantification experiments were conducted separately from the experiments where the effects of OH oxidation on WS BrC properties were examined to avoid measurement interference, as other products formed from the reaction of OH + benzoate readily absorb radiation in the same near UV region as WS BrC. As a result, the $[OH]_{ss}$ in the OH quantification experiment is lower to that of the WS BrC aging experiment, because of the presence of benzoate as an additional OH scanvenger, while the OH production rate reasons unchanged (Zhou and Mopper, 1990). As such, for the WS BrC aging experiments, the OH production rate equals to only to the consumption rate of WS BrC by OH (equation 3 where $R_{benzoate}$ = 0):

$$P_{OH} = k'_{BrC}\,[OH]_{ss} \quad (6)$$

Thus, using equation 6, for the WS BrC aging experiments, the $[OH]_{ss}$ in these experiments can be calculated from the the OH production rate and k'_{BrC} (equations 1 and 2, respectively). For these OH quantification experiments, the $[OH]_{ss}$ for solutions containing WS BrC with and without 1.5 mM H_2O_2 were determined to be 2.1×10^{-14} M and 1.55×10^{-14} M. The difference of these steady-state OH concentrations were taken to be due to the photolysis of the added 1.5 mM H_2O_2. From the reproductibility of the OH production rate for BrC with 1.5 mM H_2O_2, we estimate that the uncertainity of the $[OH]_{ss}$ is ~30%.

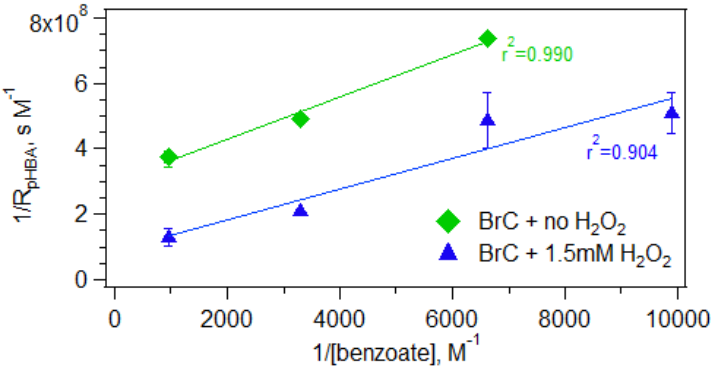

Figure S2. Relationship between the reciprocals of benzoate formation rate (R_{pHBA}) and the concentration of added benzoate in photolyzed WS wood smoke BrC solutions. Error bars represent variability (±1σ) of multiple experiments.

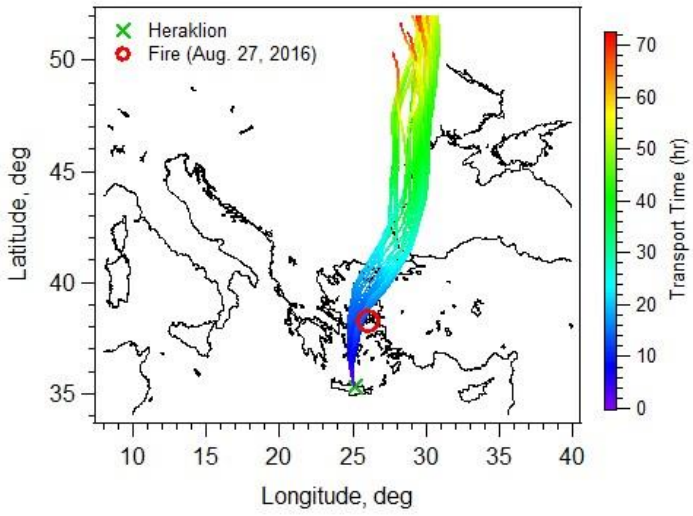

Figure S3. Multi-day biomass burning event on Chios from August 25 – 26th, 2016 (red circle) as detected by the Moderate Resolution Imaging Spectroradiometer (MODIS). Lines illustrate the 24 hourly airmass back trajectories from the sampling site (Heraklion, green cross) from July 27th, as computed using the HYSPLIT model for a total run time of 72 hours. The trace color for each line corresponds to the airmass transport time. For the field sample collected on July 27th, the estimated atmospheric transport time for the biomass burning BrC was approximately 18 hours.

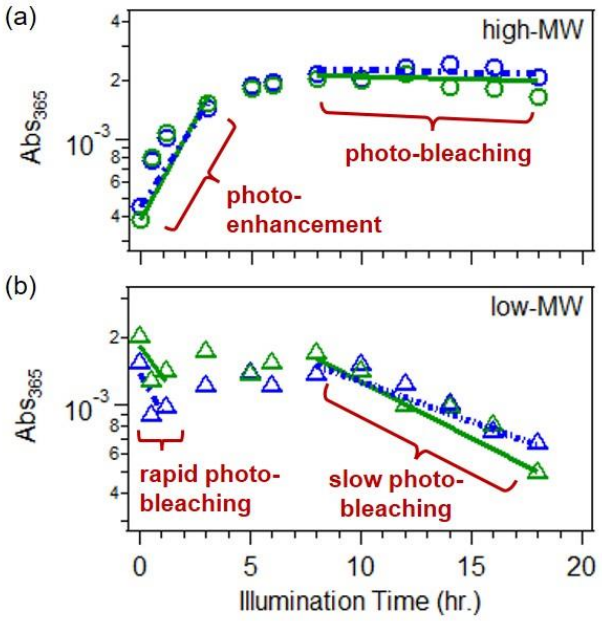

Figure S4. Light absorptivity (at 365 nm) of a) high-MW and b) low-MW WS BrC over the course of a representative experiment for aqueous OH oxidation (green) and UVB photolysis (blue). The lines illustrate the fitting of the photo-enhancement/photo-bleaching rate constants for the time periods highlighted. Note that the axis for light absorption is in log scale.

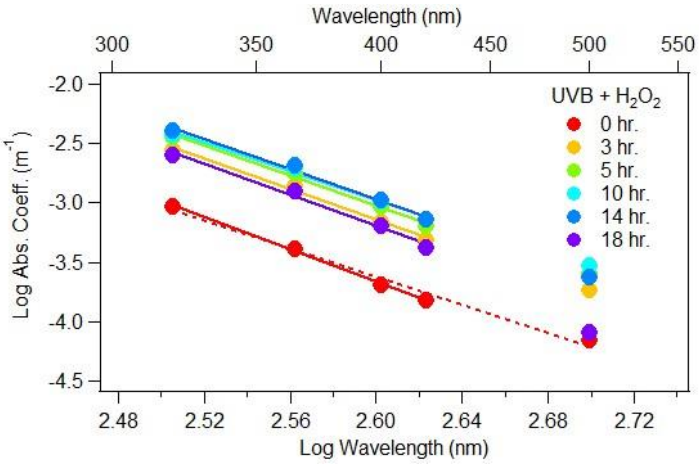

Figure S5. Log absorption coefficient vs. log wavelength over the course of a representative aqueous OH oxidation WS-BrC experiment. The linear fits determined between 320 - 420 nm (solid line) and 320 - 500nm (dash line) for BrC prior to photochemical aging (0 hr, dashed line) are illustrated.

Section 2. Atmsopheric Fate of Biomass Burning WS BrC

Aqueous OH Oxidation

The atmospheric lifetime ($\tau_{atm,\ OH\ oxd}$) due to aqueous OH oxidation (Table S1) is calculated using the experimentally determined second-order OH oxidation rate constant (k_{OH}^{II}, Table 1 in main text), and assuming a [OH]ss of 1×10^{-14} M, which represents the upper range of OH concentrations in fog/cloud droplets (Herrmann et al., 2010; Arakaki et al., 2013):

$$\tau_{atm,OH} = \frac{1}{k_{OH}^{II} \times [OH]_{ss}}$$

UV Photolysis

To estimate the atmsopheric lifetimes of processes leading to an increase (photoenhancement) and decrease (photobleaching) in the light absorptivity of different molecular weight fractions of BrC (τ_{atm}) with respective to photolysis (UVB and UVA), which are shown in Table S1, the experimentally observed lifetimes were calculated from the determined rate constants (Table 1 in main text). These observed lifetimes were converted to equivalent times in the atmosphere, assuming that the differences is only due to the ratio of photon fluxes in the photoreactor (F_{exp}) and the sun at Solar Noon (F_{atm}) in the UVB and UVA regions:

$$\tau_{atm,UV} = \tau_{exp,UV} \left(\frac{F_{\exp}}{F_{atm}}\right)$$

The photon fluxes determined for the UVB and UVA lights in the photoreactor were determined by integrating the corresponding flux (Figure S1) from 280 – 400 nm and 300 – 400 nm, respectively. For UVB lights, the photon flux ($F_{exp,\ UVB}$) was 2.57×10^{15} s^{-1} photon cm^{-2}, as determined using chemical actinometry. For UVA lights, the photon flux were determined using both chemical actinometry ($F_{exp,\ UVA,\ chemical\ actinometry}$ = 3.82×10^{16} s^{-1} photon cm^{-2}) and spectroradiometer ($F_{exp,\ UVA,\ spectroradiometer}$ = 1.51×10^{16} s^{-1} photon cm^{-2}) (Wong et al., 2017). For photon fluxes in the UVB and UVA regions from solar radiation, they were determined by integrating the flux in the same wavelength ranges mentioned above ($F_{atm,\ UVB}$ = 1.940×10^{16} s^{-1} photon cm^{-2}; $F_{atm,\ UVA}$ = 1.939×10^{16} s^{-1} photon cm^{-2}). This approach assumes that the quantum yields for BrC photoenhancement and photobleaching are wavelength independent. We also note that the calculated atmospheric lifetime with respect to photolysis assumes continuously exposure to solar photon flux corresponding to Solar Noon (i.e., no light/dark cycles).

Table S1. Estimated atmospheric lifetimes of processes leading to an increase (photoenhancement) and decrease (photobleaching) of the light absorpivity of small- and high-MW WS BrC, with respect to photolysis (UVB and UVA) and OH oxidation. Note that for UVB photolysis and OH oxiation, the rate contants for low-MW_1 and low-MW_2 photobleaching correspond to chromophores that were rapidly and slowly photobleached, respectively.

	Fraction	OH Oxidation[a]	Photolysis	
			UVB[a]	UVA[b]
BrC Photo-enhancement	Low-MW	-	-	3.2 – 8.1
	High-MW	-	1.5 ± 0.2	2.4 – 5.9
BrC Photo-Bleaching	Low-MW_1	-	0.7 ± 0.2	12 - 30
	Low-MW_2	9.8 ± 1.6	11 ± 1.6	
	High-MW	-	11 ± 2.3	14 - 36

Uncertainties in atmospheric lifetime represents the variability (±1σ) of multiple experiments (n=3).
[b] Data obtained from Wong et al., (2017) where the range of atmospheric lifetimes calculated using photon fluxes determined using chemical actinometry and measured by spectroradiometer.

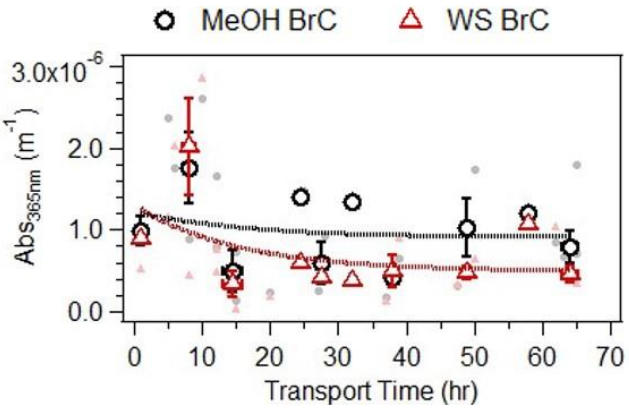

Figure S6. Fitted exponential decays to bulk light absorptivity at 365nm for MeOH (black circles) and WS (red triangles) extractable BrC in ambient biomass burning organic aerosols, sampled on Crete Island, Greece during the 2016 and 2017 fire seasons. The filled points are individual filter measurement and the open points represent the binned median values and the associated error bars represent the interquartile range.

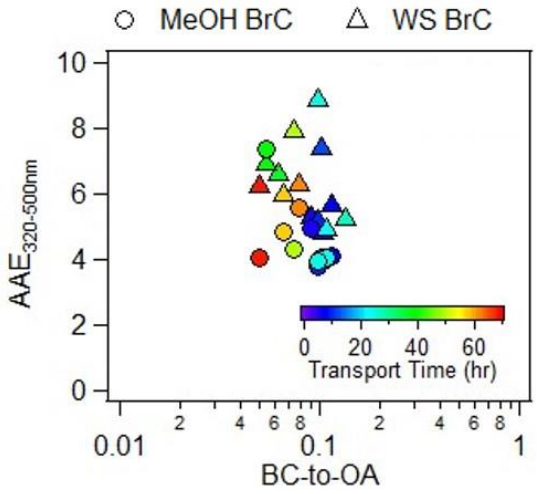

Figure S7. AAE (from 320 – 500nm) as a function of black carbon-to-organic aerosol (BC-to-OA) ratio for MeOH (circles) and water (triangles) soluble portion of the ambient filters collected on Crete, Greece during the 2017 fire season. The color scale indicates the transport time associated with each filter sample, estimated from back trajectories calculated using HYSPLIT model. OA was estimated from the measured OC concentrations, using a conversion factor of 2 (Turpin and Lim, 2001).

Table S2. Linear regression slope (*m*), coefficient of determination (r^2), and p-value (*p*) between biomass burning tracers and bulk Abs_{365} for MeOH and WS BrC). The error represents the standard deviation (±1σ) associated with the slope.[a]

	Levoglucosan	nss-K^+	Total Hydrous Sugars
MeOH BrC			
m	$(7.22 \pm 0.34) \times 10^{-9}$	**$(4.92 \pm 0.76) \times 10^{-6}$**	**$(2.88 \pm 0.30) \times 10^{-8}$**
r^2	0.00	**0.70**	**0.83**
p	0.835	**< 0.001**	**< 0.001**
WS-BrC			
m	$(9.84 \pm 0.30) \times 10^{-9}$	**$(3.68 \pm 0.87) \times 10^{-6}$**	**$(2.10 \pm 0.43) \times 10^{-8}$**
r^2	0.01	**0.50**	**0.56**
p	0.934	**< 0.001**	**< 0.001**

[a] Statistically significant correlations (p-value < 0.05) are bolded.

Reference

Anastasio, C. and McGregor, K. G.: Chemistry of fog waters in California's Central Valley: 1. In situ photoformation of hydroxyl radical and singlet molecular oxygen, Atmos. Environ., 35(6), 1079–1089, doi:10.1016/S1352-2310(00)00281-8, 2001.

Ervens, B.: Modeling the Processing of Aerosol and Trace Gases in Clouds and Fogs, Chem. Rev., 115(10), 4157–4198, doi:10.1021/cr5005887, 2015.

Herrmann, H., Hoffmann, D., Schaefer, T., Bräuer, P. and Tilgner, A.: Tropospheric Aqueous-Phase Free-Radical Chemistry: Radical Sources, Spectra, Reaction Kinetics and Prediction Tools, Chem. Phys. Chem, 11(18), 3796–3822, doi:10.1002/cphc.201000533, 2010.

Ross, A. B., Mallard, W. G., Helman, W.P., Buxton, G. V., Huie, R. and Neta, E. P.: NDRL-NIST Solution Kinetics Database - Version 2, NIST Standard Reference Data, Gaithersburg, M.D., 1994.

Turpin, B. J. and Lim, H.-J.: Species Contributions to PM2.5 Mass Concentrations: Revisiting Common Assumptions for Estimating Organic Mass, Aerosol Sci. Technol., 35(1), 602–610, doi:10.1080/02786820119445, 2001.

Wong, J. P. S., Nenes, A. and Weber, R. J.: Changes in Light Absorptivity of Molecular Weight Separated Brown Carbon Due to Photolytic Aging, Environ. Sci. Technol., 51(15), 8414–8421, doi:10.1021/acs.est.7b01739, 2017.

Zhou, X. and Mopper, K.: Determination of photochemically produced hydroxyl radicals in seawater and freshwater, Mar. Chem., 30, 71–88, doi:10.1016/0304-4203(90)90062-H, 1990.